Volume 1 | Number 1 | Jan 2013 | Pages 1–100

Journal of
Materials Chemistry C

Materials for optical and electronic devices
www.rsc.org/materialsC

ROYAL SOCIETY
OF CHEMISTRY

ROYAL SOCIETY
OF CHEMISTRY

www.rsc.org/materialsC

Journal of
Materials Chemistry C

PAPER

Multiband photoluminescence from carbon nanoflakes synthesized by hot filament CVD: towards solid-state white light sources

B. B. Wang,[a] K. Ostrikov,[b,c,] * K. Zheng,[d] L. Wang[d], and S. S. Zou[a]

[a] *College of Chemistry and Chemical Engineering, Chongqing University of Technology, 69 Hongguang Rd, Lijiatuo, Banan District, Chongqing 400054, P. R. China*
[b] *Plasma Nanoscience Centre Australia (PNCA), CSIRO Materials Science and Engineering, P. O. Box 218, Lindfield NSW 2070, Australia Email: Kostya.Ostrikov@csiro.au*
10 [c] *Plasma Nanoscience, School of Physics, The University of Sydney, Sydney NSW 2006, Australia*
[d] *Institute of Microstructure and Properties of Advanced Materials, Beijing University of Technology, Beijing 100124, P. R. China*
† Electronic Supplementary Information (ESI) available: [details of any supplementary information available should be included here]. See DOI: 10.1039/b000000x/

15
Carbon nanoflakes (CNFLs) are synthesized on silicon substrates deposited with carbon islands in methane environment using hot filament chemical vapor deposition. The structure and composition of the CNFLs are studied using field emission scanning electron microscopy, high-resolution transmission electron microscopy, micro-Raman spectroscopy, and X-ray photoelectron spectroscopy. The results indicate that the CNFLs are composed of multilayer graphitic sheets and the area and thickness of CNFs are increased with the
20 growth time. The photoluminescence (PL) of CNFLs excited by 325 nm He-Cd laser exhibits three strong bands centered at 408, 526, and 699 nm, which are related to the chemical radicals terminated on the CNFLs and the associated interband transitions. The PL results indicate that the CNFLs are promising as an advanced nano-carbon material capable of generating white light emission. These outcomes are significant to control the electronic structure of CNFLs and contribute to the development of the next-generation solid-state white light emission devices.

25
Introduction

Solid-state lighting (SSL) is a rapidly developing technology where electric power is converted into optical emission. The SSL has the advantages of high luminosity, energy-efficiency,
30 environmental friendliness, etc.[1-3] This places SSL devices among the most promising next-generation light sources.[1] White light can be obtained by combining blue, green and red emitters. However, significant energy losses and, consequently, relatively low conversion efficiency are inevitable.[4] This is why a great deal
35 of effort has recently been devoted to the development of advanced white light-emitting nanomaterials.

Existing examples of nanomaterials that directly emit white light include hybrid semiconductor materials such as 2D-$[Cd_2Se_2(ba):Te]$ (ba=bultylamine),[1] ZnO nanoparticles mixed
40 with graphene,[2] CdSe/ZnS core–shell nanocrystals hybridized with InGaN/GaN,[5] and some others. However, white light emitting nanomaterials composed of a single chemical element remain quite rare. For example, nitrogen-doped carbon films and nanodots have been reported to directly generate white light.[6,7]
45 The generation of white light may be attributed to various interband transitions[6] and size-dependent effects,[7] which is particularly strong for carbon quantum dots (commonly termed

C-dots). However, it is quite challenging to control the C-dot size which leads to the limited tunability of the luminescence and
50 quantum yield of photons.[8]

Graphene films composed of a single or a few atomic carbon layers are considered as other viable luminescent carbon nanomaterials. However, the zero bandgap of a perfect single-layer graphene sheet makes it difficult to generate
55 photoluminescence (PL).[9] On the other hand, graphene nanoflakes have a bandgap thereby showing semiconducting responses.[10,11] Likewise, there are reports that graphene oxide with a bandgap can generate PL.[12-14] One can thus expect effective generation of PL emission also from the carbon
60 nanoflakes (CNFLs), which are of primary interest of this study.

Indeed, blue emission can be generated from the aromatic or olefinic functional groups,[15] the green emission is related to the bandgap,[6] while the red PL is associated to the defect states created by oxygen.[12] Thus, the CNFLs can become the white light
65 emitting materials if they are modified by the above functional groups. The hydrocarbon radicals formed from methane under high temperatures can form the olefinic molecules.[16,17] Simultaneously, the residual oxygen in the reaction chamber can react with the CNFLs to form some oxygen-defect states. Thus,
70 the CNFLs formed in methane environment can indeed be

expected to generate white light emission. To satisfy these requirements, here we use the hot filament chemical vapor deposition (HFCVD) process to synthesize the white light emitting CNFs.

Moreover, here we employ an unconventional growth mechanism which does not rely on commonly used metal catalysts.[18] To control the CNF growth, we use carbon islands as the seeds. These seeds are pre-deposited on the mirror-polished silicon substrates by the plasma-enhanced hot filament chemical vapor deposition (PEHFCVD) using a mixture of methane, hydrogen, and nitrogen gases. The carbon islands are then used in HFCVD synthesis of the CNFLs in methane environment.

The room-temperature PL spectra show three strong PL bands centered about 408, 526 and 699 nm, which are different from the single PL bands of graphene oxide.[12-14] For the PL of graphene oxide, the different PL mechanisms are suggested, which are related to the oxygen-defect states[12] and the electron-hole pairs generated in the sp^2 islands.[13,14]

On the contrary, our CNFLs simultaneously generate three PL bands owing to the different mechanisms of photoluminescence. These PL properties are related to the morphological and structural features of the CNFLs and offer interesting opportunities for the development of next-generation white light luminescent devices.

Experimental Details

Before the synthesis of carbon nanodots and CNFLs, the organic and inorganic residues on the surfaces of silicon substrates were removed by a chemical method. To remove the organic residues, the substrates were sequentially cleaned for 15 min in toluene, acetone, and ethanol ultrasonic bath, respectively. For removing the inorganic residues, the substrates were placed into a solution composed of $NH_3 \cdot H_2O$, H_2O_2 and H_2O (with a volume ratio of 1:2:5) to boil at 75 °C for 15 min. Finally, they were washed several times in deionized water.

To synthesize the CNFLs, carbon nanodots were pre-deposited on the silicon substrates using PEHFCVD. Here, we used PEHFCVD to grow the carbon islands because low-temperature reactive plasmas are versatile in nanomaterials synthesis and processing.[8] The PEHFCVD system is similar to the system described in detail elsewhere.[19]

In the CVD reactor, the reactive gases are decomposed into the chemical radicals by the hot tungsten filaments (~1800 °C), and then the radicals are further ionized to generate positive ions by the plasma produced by a DC power supply. Because the nucleation of carbon on the mirror-polished silicon substrate can be improved by a negative bias,[20] the anode and cathode are connected to the filaments and the substrate through a molybdenum holder. The short distance of ~ 8 mm between the filaments and the substrate makes the substrate heated to about 900 °C in a short time, which is measured by a thermocouple. When the base pressure of lower than 2 Pa in the CVD reactor is reached, 20 sccm nitrogen and 80 sccm hydrogen are introduced into the CVD reactor and the pressure is adjusted to about 2×10^3 Pa. The tungsten filaments are heated by an AC power supply.

Once the substrate is heated to about 900 °C, the DC power supply is turned on to produce the plasma. After the silicon substrate is treated for 5 min in $N_2 + H_2$ plasmas, the DC power supply is turned off, and then methane is let into the CVD reactor while the flow rates of methane, nitrogen and hydrogen are adjusted to 20, 30, and 50 sccm, respectively. At the same time, the DC power supply is turned on again and the bias current is then set to 160 mA to deposit the carbon nanodots for 15 min.
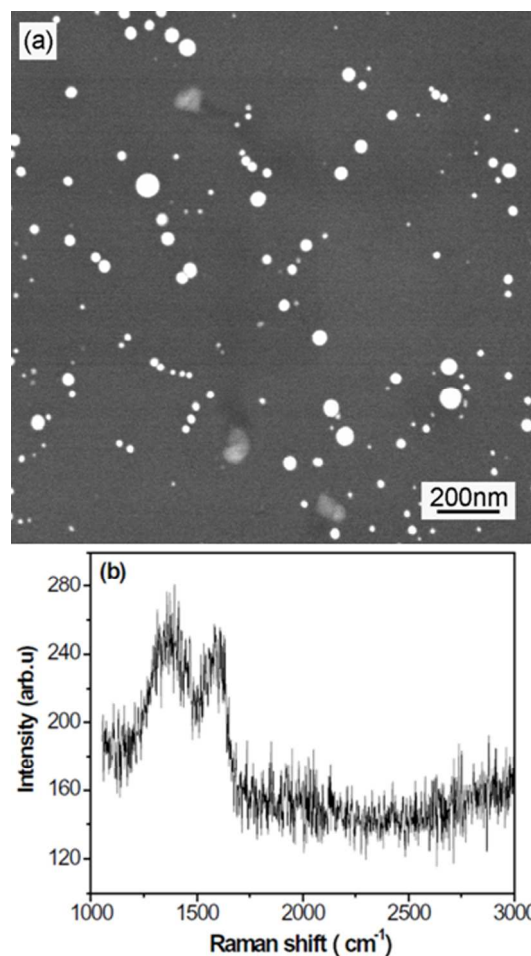

Fig. 1 FESEM image and Raman spectrum of carbon islands deposited on a silicon substrate (a): FESEM image; (b): Raman spectrum.

The CNFLs are then synthesized in the HFCVD system, where the synthesis procedure is quite similar to the deposition of the carbon islands described above. After the CVD reactor is pumped down to a base pressure of lower than 2 Pa, 50 sccm hydrogen is introduced into the CVD reactor and the pressure is adjusted to 2×10^3 Pa. When the substrate temperature reaches about 930 °C, the hydrogen gas flow controller is turned off. Simultaneously, the 50 sccm methane flow is quickly let into the CVD reactor to grow the CNFLs. In this series of experiments, three specimens A-C are prepared in the processes that lasted 4, 6, and 8 min, respectively.

The morphological features of the CNFLs are investigated by a Hitachi S-4800 field emission scanning electron microscopy (FESEM) operated with 15 kV electron beam accelerating voltage. The chemical structure of the CNFLs is analyzed using a JEOL 2010F transmission electron microscope (TEM) operated at 200 kV. The composition of CNFLs is studied by a HR 800 micro- Raman spectroscopy using a 532 nm line of a
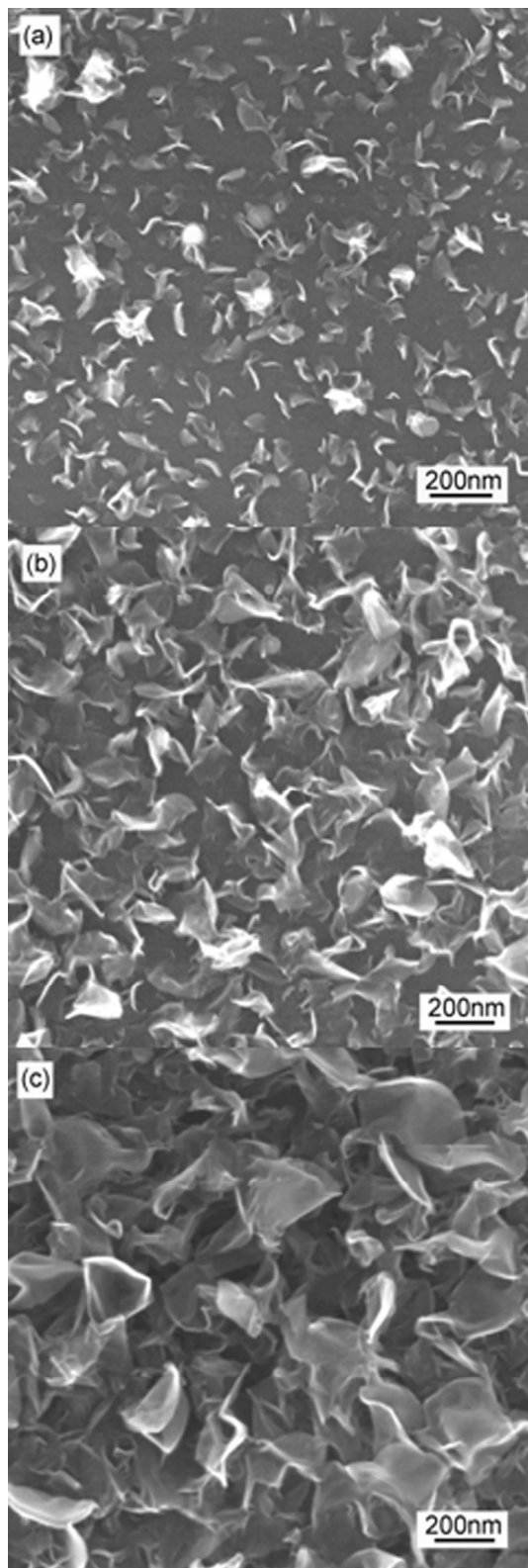
Fig. 2 FESEM images of specimens A-C (a): A; (b): B; (c): C.

semiconductor laser as the excitation source, a ESCALAB 250 X-ray photoelectron spectroscopy (XPS) using an Al Kα X-ray source, and a 8400S Shimadzu Fourier transform infrared (FTIR) spectroscopy, respectively. The PL of CNFLs is measured in the

HR 800 micro-Raman system, where a 325 nm line of a He-Cd laser was used as the excitation source; the power of the laser was set to 10 mW.

Results and discussion

Structure and composition of CNFLs

Figure 1 is the FESEM image and Raman spectrum of the carbon islands deposited on the silicon substrate. As shown in Fig. 1(a), the carbon islands are non-uniformly distributed on the silicon surface and their diameter is also non-uniform. According to the results obtained by a standard digital image processing of the relevant SEM images, the diameter of the typical carbon islands is within the 10-80 nm range. Figure 1(b) shows two Raman peaks at about 1373 and 1600 cm^{-1}, which are the common D and G peaks of sp^2 carbon nanomaterials, respectively.[21]

Figure 2 shows the FESEM images of specimens A-C. From Fig. 2, one can see that the area of CNFLs becomes larger from specimen A to specimen C, which indicates that the CNFLs increase in size with growth time.
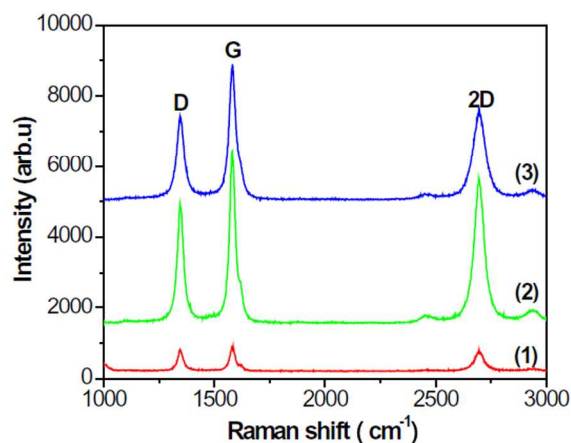
Fig. 3 Raman spectra of specimens A-C (1): A; (2): B; (3): C.

Figure 3 presents the Raman spectra of specimens A-C, which shows the D, G, and 2D peaks at about 1343, 1580, and 2696 cm^{-1}, respectively. From Fig.3, the intensity ratio of G to D peak is about 1.2, 1.4 and 1.7, respectively, which means that the G peak is stronger than the D peak. The strong G and 2D peaks indicate that the CNFLs are composed of a few graphene sheets.[22] The ratio of intensities of 2D and G peaks deduced from Fig. 3 is about 0.85, 0.82, and 0.65 for the spectra (1)-(3), respectively. These data suggest that the CNF thickness gradually increases with the growth time as evidenced by the lower ratio of the intensities of the 2D and G peaks as the number of graphene sheets becomes larger.[23]

Due to the similarity of Raman spectra of the specimens, specimen B is investigated by TEM after the CNFLs were scraped from the silicon substrate using a sharp knife and the results are shown in Fig. 4. From the high-resolution TEM image in Fig. 4(b), one can see regular graphitic sheets. We used Digital Micrograph software (Gatan^{TM}) to obtain the width of 10 carbon
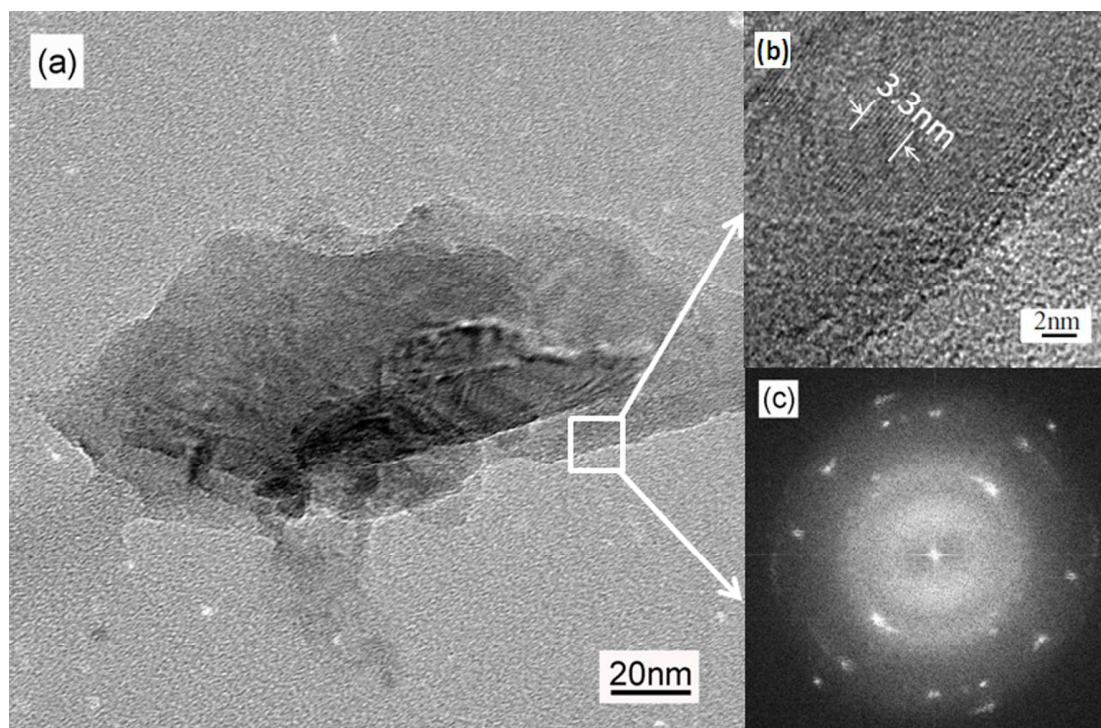
Fig. 4 TEM and FFT images of the specimen B (a): TEM; (b): high-resolution TEM; (c): FFT image.

sheets and found it to be equal to 3.3 nm, giving the 0.33 nm spacing between two carbon sheets, which clearly corresponds to the interlayer spacing of graphite (0.335 nm).[24] In Fig. 4(c), the fast Fourier transform (FFT) image shows two families of spots, which indicate that the CNFLs are composed of only a few graphene sheets.[25] Simultaneously, Fig.4(c) shows the weak diffusive rings, which most likely originate due to the presence of amorphous carbon on the microgrid used for holding the TEM specimen. A quite similar pattern has previously been reported for multilayer graphene sheets.[26]

To further confirm the composition of CNFLs, specimen A was analyzed by XPS. Figure 5 shows the XPS spectra of specimen A. The wide XPS spectrum in Fig. 5(a) shows the *C* 1s and *O* 1s XPS peaks at about 283.98 and 532.46 eV, respectively. The very weak peak at 532.46 eV implies that there is a very small amount of oxygen in the CNFLs, with the oxygen content of about 0.8 at% according to the XPS measurement results. Figures 5(b) and (c) represent the C *1s* and O *1s* XPS spectra. For the analysis of bonding states of the elements, the C *1s* and O *1s* XPS spectra are fitted by the standard XPS fitting software after Shirley background subtraction. As shown in Fig. 5(b), the C *1s* peak is fitted by two peaks at about 283.97 and 284.79 eV, which are attributed to the Si-C and sp^2 C-C bonds, respectively.[27,28] For the O *1s* peak, it is decomposed into two peaks at about 531.44 and 532.46 eV, respectively. The peak at ~531.44 eV is related to the C=O bonds while the peak at ~532.46 eV is associated with the C-O-H and/or C-O-C bonds.[29]

In Fig. 5(b), one can see that the peak related to silicon carbide is stronger than the sp^2 carbon peak, which is related to the formation of CNFLs from the carbon islands. The growth time of specimen A is the shortest among the three specimens, thus the area of CNFLs is small, which is confirmed by Fig. 2. When the hydrocarbon radicals are deposited on the silicon surface, they react with silicon to from silicon carbide. Due to the small area of CNFLs, most of the substrate surface contributes to the XPS measurement. As a result, the peak related to silicon carbide appears stronger than the sp^2 carbon peak.

In the XPS spectra, the appearance of the carbon oxide peak results from the residual oxygen in the CVD reactor. During the growth of CNFLs, oxygen gas is not employed, thus the above peak originates from the residual gases in the CVD reactor. Because oxygen is an active element, it easily reacts with carbon to form carbon oxide. However, the residual oxygen content is small so that the peak related to oxygen is weak.

The XPS spectrum in Fig. 5 (c) shows the peaks related to the C=O, C-O-H, and C-O-C bonds. To further confirm the functional groups related to these bonds, the specimen C was studied by FTIR and the result is shown in Fig. 6. In Fig. 6, the peak at about 624 cm^{-1} is assigned to out-of-plane C-H deformation vibrations,[30] the peaks at 1382 and 1620 cm^{-1} are attributed to the C-O-C and C=C groups, respectively,[31] the peak at about 2345 cm^{-1} is related to the CO_2 group,[32] and the peaks at 3406-3555 cm^{-1} are associated with the presence of –OH groups.[33]

Possible role of carbon islands in CNFL growth

Before the growth of CNFLs, we pre-deposit the carbon islands on the silicon surfaces to promote the formation of CNFLs. The pre-deposition of carbon islands play two possible

roles in the CNFL growth. One is the acceleration of the reactions among the hydrocarbon radicals because the carbon black can be used to catalyze the decomposition of methane;[34] the other is the
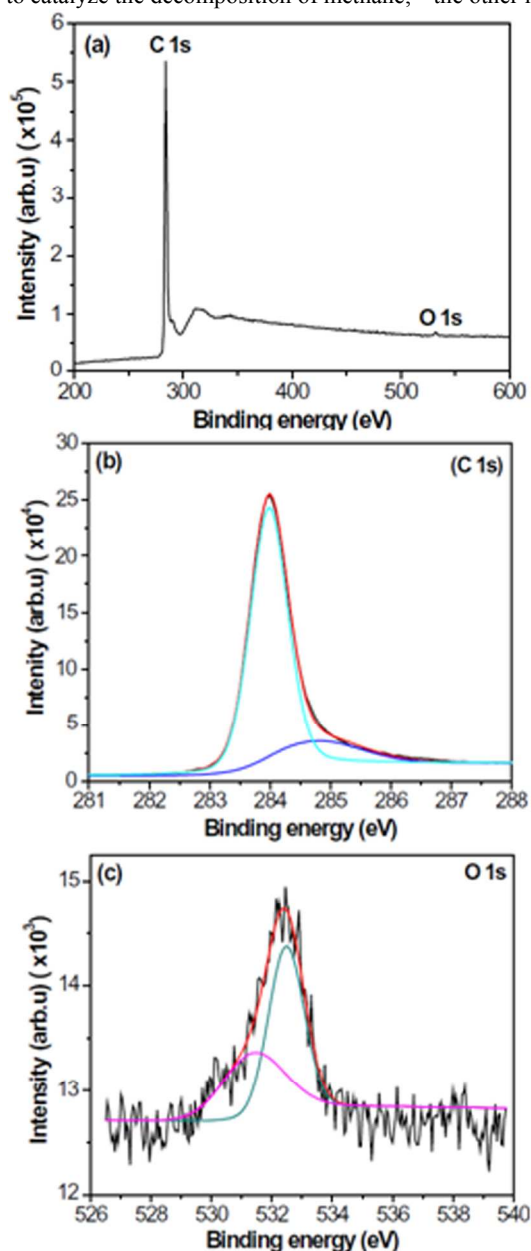

Fig. 5 XPS spectra of specimen A (a): XPS wide spectrum; (b): *C* 1s XPS spectrum; (c): *O* 1s XPS spectrum.

lowering of the energy for carbon nucleation due to the formation of the pit-like defects at the joints of the islands with silicon surface.[20]

During the synthesis of CNFLs, methane is decomposed into various hydrocarbon radicals by the hot filaments,[35] with the initial products methyl radicals and atomic hydrogen to form via the following reaction,[16]

$$CH_4 \rightarrow CH_3 + H. \qquad (1)$$

Of course, methane cannot be completely decomposed by the hot filaments due to the continuous gas flow. When the hydrogen, methyl radicals, and methane molecules reach the silicon surface, methane reacts with hydrogen to form the methyl radial through
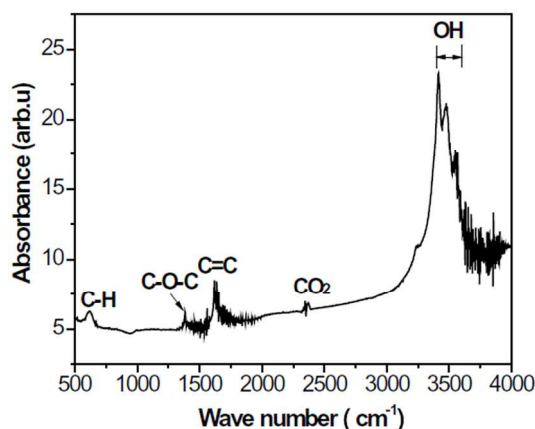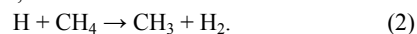
the following reaction,[16]

$$H + CH_4 \rightarrow CH_3 + H_2. \qquad (2)$$

Fig. 6 FTIR spectrum of specimen C

On the silicon surface, the methyl radicals form the ethylene molecules through a series of reactions,[16] then ethylene molecules form benzene molecules,[36] which in turn contribute to the CNFL formation. Because the carbon black can accelerate the decomposition of methane, it can accelerate the reaction of hydrocarbon radicals so that the CNFLs can be fast formed on the surfaces of carbon islands. One can thus say that the carbon islands promote the formation of CNFLs and this is why Fig. 2(a) shows that there are more CNFLs near the carbon islands than elsewhere.

Due to the carbon islands, the pit-like defects are formed at the joints of the carbon islands with the silicon surface. Recent study revealed that lower energy is required for carbon nucleation in a pit relative to a plain surface.[20] Thus, the nucleation of CNFLs requires a low energy at the joints of the islands with silicon surface, i.e., the growth of CNFLs starts from the carbon islands. This is another reason that the carbon islands can indeed promote the formation of CNFLs.

Here we emphasize that the use of high concentration of methane as carbon source for the carbon island synthesis was possible in this work, in part due to the ability of the hot-filament-produced plasmas to effectively dissociate precursor molecules. In addition, the plasma can be used to grow a number of other nanomateials such as various metal oxide nanostructures including nanowires.[37-40]

It is also worth mentioning that our method of the CNFLs growth is quite simple because it is catalyst-free and no further treatment is required for the PL study. This is an obvious advantage compared to other works,[12,18] where catalyst was deposited using a sputtering system while further oxygen plasma treatment was needed to prepare the specimens for the PL analysis.

PL properties of CNFLs

Figure 7 shows the PL spectra of CNFLs obtained from different places on the surfaces of specimens A-C, which show three PL bands centered about 408, 526, and 699 nm, respectively. The same peak position for every corresponding band in Figs. 7(a) and (b) indicates that the PL emission is generated from the

CNFLs. Previously, the PL properties of graphene-based nanomaterials were studied.[12-14] Gokus *et al*. proposed that the PL generation of graphene oxide is related to the defect states induced by oxygen,[12] while Eda and Luo *et al*. suggested that the PL in graphene is associated with the band emission from electron-confined sp^2 carbon islands.[13,14] However, Shen *et al*. attributed the strong PL emission of graphene quantum dots to the surface-passivation effects.[41] In addition, a combination of graphene quantum dots with agar and zinc oxide quantum dots as the conversion materials helped converting blue emission into white light. The generation of blue light is attributed to the functional groups on the surfaces of graphene quantum dots and the electron transition between the *O* 2p state of zinc oxide quantum dots and the unoccupied state of graphene oxide, respectively.[42,43] Guo and coworkers[44] studied the photoinduced electron transfer between pyridine coated cadmium selenide quantum dots and single-sheet graphene and found that the single-sheet graphene can quench the emission of quantum dots.

In these studies, the PL properties of monolayer graphene, graphene quantum dots or their hybrids were studied. In particular, a sole PL band was detected,[12-14] implying that the mechanism of PL in our case may be quite different. Indeed, the simultaneous excitation of three PL bands suggests the co-existence of multiple mechanisms of photoluminescence in our CNFL samples.
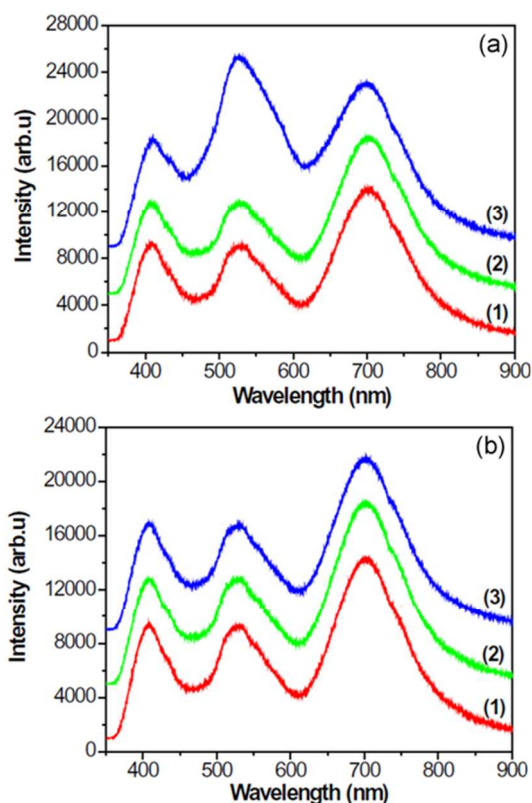
Fig.7 PL spectra of GFs obtained from different places on the specimen surfaces (1): A; (2): B; (3): C.

For our specimens, the CNFLs are composed of multilayer graphene. If the PL generation is interpreted using the radiative recombination of electron-hole pairs produced in the sp^2 clusters by photo-induction, the size of clusters should be about 1 nm.[45] Since the thickness of CNFLs in Fig.2 is about 8 nm, it is impossible to generate the PL through radiative recombination of electron-hole pairs produced in the sp^2 carbon clusters. Previous results suggest that the bandgap of ~3 nm sp^2 carbon clusters is about 0.5 eV, with the corresponding wavelength of 2480 nm.[13] For the CNFLs in our specimens, the bandgap is lower than 0.5 eV because the bandgap is reduced with the increase in the size of sp^2 carbon clusters,[13] thus it is unlikely to attribute our results to the bandgap emission.

The research results of Fanchini *et al*. indicate that the energy gap of π^* and π states of carbon materials is ~2.5 eV although their optical gap is lower than 1 eV.[46] Other authors[6] used the interband transition mechanism to explain the PL generation of carbon materials according to the state density model. In this model the PL bands of more than 2 eV originate from the transition between the π^* and π bands, or the transition between the σ^* band and the valence band formed by defects, while the transition between the π^* band and the valence band formed by defects occurs in the energy range below 2 eV. The transition mechanism was also used to interpret the generation of multiple PL bands.[43] Furthermore, the results of Chiou *et al*. indicate that the PL generation of graphene nanoflakes is related to the induced changes of the electronic structure and the presence of disorder-induced localized states in the region of π states and the gap between the π^* and π states.[47] In addition, the PL generation is related to the function group and defects.[12,15,42] These PL mechanisms will be used below to interpret the PL generation in our experiments.

From the above analyses, we note that hydrocarbon (e.g., methyl, ethenyl) radicals can be formed during the growth of CNFLs. When the growth of CNFLs stops, these radicals can terminate the edges and also possibly the surfaces of the CNFLs because they are easily bonded to benzene.[48] Because blue PL can be generated from the aromatic or olefinic molecules,[15] the blue PL band centered about 408 nm is attributed to the ethenyl radicals on the CNFLs. The energy corresponding to 408, 526, and 699 nm is 3.05, 2.36 and 1.78 eV, respectively. The energy gap of π^* and π states of carbon materials is ~2.5 eV.[46] According to the interband transition mechanism,[6] the blue PL band can originate from the transition between σ^* and π bands.

Figure 2 also reveals that the CNFLs are morphologically and structurally similar to the vertical graphene sheets[8,11] which also have a bandgap. Thus, the green PL band centered about 526 nm can indeed be attributed to the transition between the π^* and π bands.[6] Figures 5(c) and 6 indicate the formation of C-O bonds, i.e., there are the defect states formed within the π^* and π bands.[12] The red PL band centered about 699 nm is related to the transition between the π^* band and the oxygen-defect states.

Figure 3 indicates that the CNFLs vary in thickness which in turn leads to the bandgap variation among different structures. As a result, the intensity of PL bands also varies among the specimens and the measurement spots shown in Fig. 7. The PL efficiency trends are similar to the results of other authors.[49]

The Commission Internationale de L'eclairage (CIE) chromaticity coordinate diagram for the white light emission is presented in Fig. 8. The CIE chromaticity coordinates of the specimens are calculated according to the following

equations:[51,52]

$$x = \frac{0.49000r + 0.31000g + 0.20000b}{0.66697r + 1.13240g + 1.20063b}, \quad (3)$$

$$y = \frac{0.17697r + 0.81240g + 0.01063b}{0.66697r + 1.13240g + 1.20063b}, \quad (4)$$

$$z = \frac{0.00000r + 0.01000g + 0.99000b}{0.66697r + 1.13240g + 1.20063b}, \quad (5)$$

$$r = \frac{R}{R + G + B}, \quad (6)$$

$$g = \frac{G}{R + G + B}, \quad (7)$$

$$b = \frac{B}{R + G + B}, \quad (8)$$

where *R, G, B* are the stimulus values of red, green and blue light. From Fig.7, the intensity of red, green and blue light is obtained. According to Eqs.(3)-(8), the CIE chromaticity coordinates are calculated to be 0.377 and 0.322 for the spectra (1) and (2) in Fig. 7(a) and spectra (1)-(3) in Fig. 7(b). These coordinates are 0.359 and 0.405 for the spectrum (3) in Fig. 7(a). The two coordinate points are shown in Fig.8, which are marked in circle (A) and triangle (b) shapes, respectively. As shown in Fig.8, the two points are located in the region of white light emission, which imply that the CNFLs can be used for the development of white light sources. Our results show that the CNFLs can emit the white light, which indicates that carbon nanomaterials represent a viable alternative to inorganic compound nanomaterials. More importantly, the CNFs can be regarded as a promising source of white light emission.
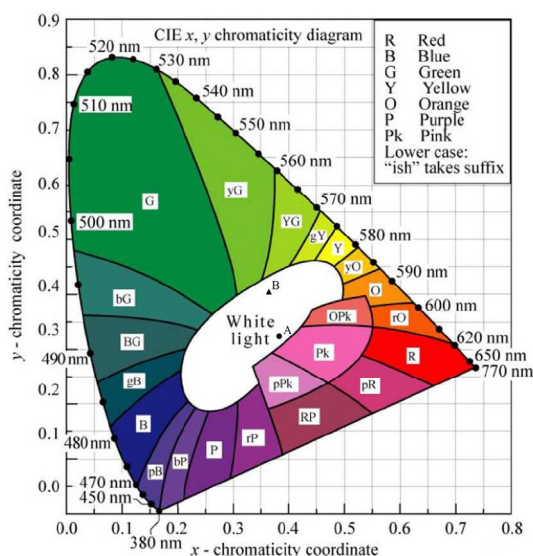

Fig. 8 CIE 1931 *x,y* chromaticity diagram (reprinted with permission from Ref. (50))

Conclusion

In summary, CNFLs were synthesized on silicon substrates by HFCVD and their structure and composition were studied using FESEM, high-resolution TEM, micro-Raman spectroscopy,

and XPS analyses. The results indicate that the area and thickness of CNFLs increase with the growth duration.

The photoluminescence studies confirm that the CNFLs can generate three strong PL bands centered about 408, 526, and 699 nm. These bands are attributed to the chemical radicals terminated on the CNFs and the transitions between the σ* and π bands, between the π* and π bands, and between the π* band and the oxygen-defect states, respectively. The simultaneous generation of the blue, green and red photoluminescence bands indicates that the CNFLs can be regarded as effective sources of white light emission. These results advance our knowledge of the growth and optoelectronic properties of graphene-based materials and contribute to the development of the next-generation solid-state white light emission devices.

Notes and References

1 W. Ki, J. Li, G. Eda, M. Chhowalla, *J. Mater. Chem.,* 2010, **20**, 10676.

2 P. Kumar, L. S. Panchakarla, S. V. Bhat, U. Maitra, K. S. Subrahmanyam, C. N. R. Rao, *Nanotechnol.,* 2010, **21**, 385701.

3 S. Ye, F. Xiao, Y. X. Pan, Y. Y. Ma, Q. Y. Zhang, *Mater. Sci. Eng.,* 2010, **R71**, 1.

4 A. H. Mueller, M. A. Petruska, M. Achermann, D. J. Werder, E. A. Akhadov, D.l D. Koleske, M. A. Hoffbauer, V. I. Klimov, *Nano Lett.,* 2005, **5**, 1039.

5 S. Nizamoglu, T. Ozel, E. Sari, H. V. Demir, *Nanotechnol.,* 2007, **18**, 065709.

6 Y. Iwano, T. Kittaka, H. Tabuchi, M. Soukawa, S. Kunitsugu, K. Takarabe, K. Itoh, *Jpn. J. Appl. Phys.* 2008, **47**, 7842.

7 W. Kwon, S. Do, J. Lee, S. Hwang, J. K. Kim, S.-W. Rhee, *Chem. Mater.,* 2013, **25**, 1893.

8 K. Ostrikov, E. C. Neyts, M. Meyyappan, *Adv. Phys.,* 2013, **62**, 113.

9 L. Caro, M. J. Meziani, S. Sahu, Y. P. Sun, *Acc. Chem. Res.,* 2013, **46**, 171.

10 M. Y. Han, B. Özyilmaz, Y. Zhang, P. Kim, *Phys. Rev. Lett.,* 2007, **98**, 206805.

11 D. H. Seo, S. Kumar, K. Ostrikov, *Carbon,* 2011, **49**, 4331.

12 T. Gokus, R. R. Nair, A. Bonetti, M. Böhmler, A. Lombardo, K. S. Novoselov, A. K. Geim, A. C. Ferrari, A. Hartschuh, *ACS Nano,* 2009, **3**, 3963.

13 G. Eda, Y.-Y. Lin, C. Mattevi, H. Yamaguchi, H.-A. Chen, I-S. Chen, C.-W. Chen, M. Chhowalla, *Adv. Mater.,* 2010, **22**, 505.

14 Z. Luo, P. M. Vora, E. J. Mele, A. T. C. Johnson, J. M. Kikkawa, *Appl. Phys. Lett.,* 2009, **94**, 111909.

15 F. Bonaccorso, Z. Sun, T. Hasan, A. C. Ferrari, *Nature Photonics,* 2010, **4**, 611.

16 C.-J. Chen, M. H. Back, R. A. Back, *Can. J. Chem.* 1976, **54**, 3175.

17 D. B. Murphy, R. W. Carroll, J. E. Klonowski, *Carbon,* 1997, **35**, 1819.

18 Y. Wu, P. Qiao, T. Chong, Z. Shen, *Adv. Mater.,* 2002, 14, 64.

19 B. B. Wang, Q. J. Cheng, X. X. Zhong, Y. Q. Wang, Y. A. Chen, K. Ostrikov, *J. Appl. Phys.,* 2012, **111**, 044317.

20 B. B. Wang, W. L. Wang, K. J. Liao, J. L. Xiao, *Phys. Rev.,* 2001, **B 63**, 085412.

21 A. C. Ferrari, J. Robertson, *Phys. Rev.,* 2001, **B 64**, 075414.

22 A. C. Ferrari, J. C. Meyer, V. Scardaci, C. Casiraghi, F. Mauri, S. Piscanec, D. Jiang, K. S. Novoselov, S. Roth, A. K. Geim, *Phys. Rev. Lett.,* 2006, **97**, 187401.

23 X. Li, W. Cai, J. An, S. Kim, J. Nah, D. Yang, R. Piner, A. Velamakanni, I. Jung, E. Tutuc, S. K. Banerjee, L. Colombo, R. S. Ruoff, *Sci.,* 2009, **324**, 1312.

24 G. Srinivas, Y. Zhu, R. Piner, N. Skipper, M. Ellerby, R. Ruoff, *Carbon,* 2010, **48**, 630.

25 G. Jo, M. Choe, C-Y. Cho, J. H. Kim, W. Park, S. Lee, W.-K. Hong, T.-W. Kim, S.-J. Park, B. H. Hong, Y. H. Kahng, T. Lee, *Nanotechnol.,* 2010, **21**, 175201.

26 C. Virojanadara, M. Syväjarvi, R. Yakimova, and L. I. Johansson, *Phys. Rev.,* 2008, B78, 245403

27 A. Fink, W. Widdra, W. Wurth, C. Keller, M. Stichler, A. Achleitner, G. Comelli, S. Lizzit, A. Baraldi, D. Menzel, *Phys. Rev.,* 2001, **B 64**, 045308.

28 M. H. Ahmed, J. A. Byrne, J. McLaughlin, W. Ahmed, *J. Biomater. Nanobiotechnol.,* 2013, **4**, 194.

29 Z. R. Yue, W. Jiang, L. Wang, S. D. Gardner, C. U. Pittman Jr., *Carbon,* 1999, **37**, 1785.

30 B. Schwenzer, S. N. Kerisit, M. Vijayakumar, *RSC Adv.,* (in press, DOI: 10.1039/C3RA46069J)

31 E. Fuente, J. A. Menéndez, M. A. Díez, D. Suárez, M. A. Montes-Morán, *J. Phys. Chem.,* 2003, **B 107**, 6350.

32 C. Matranga, L. Chen, M. Smith, E. Bittner, J. K. Johnson, B. Bockrath, *J. Phys., Chem.,* 2003, **B** 107, 12930.

33 P.-C. Hsu, H.-T. Chang, *Chem. Commun.,* 2012, **48**, 3984.

34 S. C. Lee, H. J. Seo, G. Y. Han, *Korean J. Chem. Eng.,* 2013, **30**, 1716.

35 M. Younessi-Sinaki, E. A. Matida, F. Hamdullahpur, *Int. J. Hydrogen Eng.,* 2009, **34**, 3710.

36 Becker, K. J. Hüttinger, *Carbon,* 1998, **36**, 177.

37 G. Arnoult, T. Belmonte, and G. Henrion, *Appl. Phys. Lett.,* 2010, **96**, 101505.

38 U. Cvelbar, Z. Chen, M. K. Sunkara, and M. Mozetic, *Small,* 2008, **4**, 1610.

39 S. Sharma and M. K. Sunkara, *J. Am. Chem. Soc.,* 2002, **124**, 12288.

40 M. Mozetic, U. Cvelbar, M. K. Sunkara, and S. Vaddiraju, *Adv. Mater.*, 2005, **17**, 2138.

41 J. Shen, Y. Zhu, X. Yang, J. Zong J. Zhang, C. Li, *New J. Chem.,* 2012, **36**, 97.

42 C. M. Luk, L. B. Tang, W. F. Zhang, S. F. Yu, K. S. Teng, S. P. Lau, *J. Mater. Chem.,* 2012, **22**, 22378

43 D. I. Son, B. W. Kwon1, D. H. Park, W.-S. Seo, Y.j. Yi, B. Angadi, C.-L. Lee, W. K. Choi, *Nat. Nanotechnol.* 2012, **7**, 465.

44 S. Guo, D. Bao, S. Upadhyayula, W. Wang, A. B. Guvenc, J. R. Kyle, H. Hosseinibay, K. N. Bozhilov, V. I. Vullev, C. S. Ozkan, M. Ozkan, *Adv. Funct. Mater.,* 2013, **23**, 5199.

45 M. Füle, J. Budai, S. Tóth, M. Veres, M. Koós, *J. Non-Cryst. Solids,* 2006, **352**, 1340.

46 G. Fanchini, G. Messina, A. Paoletti, S. C. Ray, S. Santangelo, A. Tagliaferro, A. Tucciarone, *Surf. Coat. Technol.,* 2002, **151-152**, 257.

47 J. W. Chiou, S. C. Ray, S. I. Peng, C. H. Chuang, B. Y. Wang, H. M. Tsai, C. W. Pao, H.-J. Lin, Y. C. Shao, Y. F. Wang, S. C. Chen, W. F. Pong, Y. C. Yeh, C. W. Chen, L.-C. Chen, K.-H. Chen_, M.-H. Tsai, A. Kumar, A. Ganguly, P. Papakonstantinou, H. Yamane, N. Kosugi, T. Regier, L. Liu, T. K. Sham, *J. Phys. Chem.,* 2012, **C 116**, 16251.

48 J. MuMurry, Organic Chemistry, Wadsworth, Inc, Belmont, CA, 1984.

49 J. Robertson, *Phys. Rev.,* 1996, **B 53**, 16302.

50 E. F. Schubert, Light-Emitting Diodes, Cambridge University Press, 2006.

51 H. S. Fairman, M. H. Brill, H. Hemmendinger, *Color Res. Appl.,* 1997, **22**, 11.

52 X. R. Xu, M. Z. Su, Luminescence and Luminescent Materials, Chemical Industry Press, Beijing, 2004 (in Chinese).